VOL. 16, NO. 9, MAY 2021 ISSN 1819-6608
ARPN Journal of Engineering and Applied Sciences

www.arpnjournals.com

# 1-D SIMULATION OF THE CHARACTERISTICS OF FUEL PRESSURE PULSATIONS AND INJECTED FUEL MASS VARIATIONS CAUSED BY A HIGH-PRESSURE GDI PUMP OPERATION

Choong Hoon Lee
Department of Mechanical and Automotive Engineering, Seoul National University of Science and Technology, Seoul, Korea
E-Mail: chlee5@seoultech.ac.kr

**ABSTRACT**

In general, a GDI (gasoline direct injection) engine uses a single-piston type of high-pressure fuel pump (HPFP) driven by a camshaft. When the HPFP that pressurizes the fuel by a reciprocating piston operates, the pressure of the delivered fuel pulsates. If the fuel rail pressure (FRP) pulsation increases past a certain point, the fluctuation of the fuel injection rate also increases and the parts may be damaged. The FRP pulsation induced by a HPFP was computer simulated. The mitigation effect of the FRP pulsation with an orifice connecting the HPFP outlet and the fuel rail was investigated. Fuel pressure waves at both the HPFP outlet and the fuel rail were simulated according to changes of the opening and closing timing of a PCV (pressure control valve) in the HPFP. The signal-to-noise ratio from the simulated pressure wave was calculated. The fuel injection rate was also simulated. Three cases of fuel rail pressure conditions were used in the simulation: 50, 100, and 150 bar. In addition, four different engine speed conditions were used: 1500, 3000, 4500, and 6000 rpm. Three orifice diameters were also used: 0.75, 1.0, and 1.5 mm. When the PCV opening time came before the TDC and the engine speed was high, the pressure pulsation and injected fuel mass variation were appeared to belarge. When the PCV opening time was later than the TDC, there was no pressure pulsation and little variation in the injected fuel mass for all simulation condition.

**Keywords:** gasoline direct injection, fuel rail pressure, pressure control valve, pressure pulsation, 1-D simulation.

## INTRODUCTION

Unlike the PFI (port fuel injection) method, which injects fuel into the intake port, the GDI method injects fuel directly into the cylinder. In the PFI system, as soon as fuel is injected into the intake port, the fuel evaporates and mixes with the intake air instantly. This effectively mixes the fuel and air. The GDI method injects high-pressure fuel into compressed fresh air, which somewhat hinders the mixing of the fuel and the air [1-4]. The GDI method has the effect of cooling the combustion chamber by the latent heat of evaporation of the fuel, thereby increasing the volumetric efficiency. This cooling effect also compensates for the decrease in the pure air partial pressure due to the increased fuel vapor partial pressure [5]. Cooling of the intake air by GDI has the effect of suppressing knocking, which can increase the compression ratio of the engine. A high compression ratio can result in both improved fuel economy and increased torque of the engine [6]. With a GDI engine, engine downsizing is possible because this engine can achieve greater torque than a PFI engine at the same displacement. Currently, most passenger vehicles are equipped with GDI engines [7].

Despite the improvements in fuel efficiency and in reducing engine sizes, which are the advantages of a GDI engine, GDI engines are associated with the disadvantages of the difficult mixing of the fuel and air quickly in the cylinder and lean control of the air-fuel ratio. These issues lead to excessive emissions of soot, difficulty in removing NOx, complex fuel injection control systems, and noise and vibration caused by reciprocating fuel pumps [8, 9]. The air-fuel mixing characteristic in the cylinder affects the combustion characteristics. This affects the engine performance and emissions [10]. In recent years, the issues of particulate matter (PM) emissions from GDI engines have been highlighted. This has led to strengthened regulations around the world to reduce PM emissions from GDI engines [10]. In order to overcome these drawbacks of GDI engines and develop a high-performance engine, it is necessary to study the GDI fuel system and its components.

The most influential factor with regard to the performance of a GDI engine is the fuel injection system. The GDI fuel injection system consists of a low-pressure pump, a HPFP, a fuel rail, and injectors. Of these, the HPFP, injector, and fuel rail have a particularly significant impact on the engine performance. By driving a low-pressure fuel pump in the fuel tank, the fuel is sent to the inlet of the HPFP. The fuel supplied to the HPFP is compressed in the upstroke of the HPFP reciprocating piston and the high-pressure fuel is delivered to the fuel rail. At this time, the opening and closing timing of the PCV in the HPFP greatly affect the fuel rail pressure and its pulsation. The fuel rail pressure pulsation increases the rail pressure amplitude, resulting in failures of components that make up the injection system, injection rate variations, and HPFP noise. The influence of the HPFP on the fuel rail pressure pulsation and noise was studied and simulated by several researchers [11-13]. However, these studies were very limited with regard to rail pressure pulsation and fuel injection rate variations.

In the present study, a 1-D simulation of a fuel rail pressure wave from a single-piston type HPFP driven by a square cam was performed. An orifice was installed between the HPFP outlet and the fuel rail to relieve the pulsation of the HPFP outlet pressure. The effect of the

orifice diameter on the fuel rail pressure pulsation and the injected fuel mass variation was simulated. The effects of the opening and closing timing of the PCV on the fuel pressure pulsation and injected fuel mass variations at both the HPFP outlet and fuel rail were simulated. The software used in the simulation is GT-Suite.

**GDI Fuel Injection System for Computer Simulation**

The internal structure of the HPFP is shown in Figure-1. Figure-1 is a modification of the GDI HPFP schematic of Spegar *et al.* [11]. Because a square cam is used, each time the camshaft makes one revolution, and the HPFP compresses the fuel four times. Figure-2 shows the square cam lift profile. There are four peaks in the cam lift profile per revolution of the camshaft. When the PCV plate of the HPFP moves to the left by the activation of the solenoid, the fuel fed into the pumping chamber is pressurized when the plunger rises with the cam profile. When the solenoid is deactivated and the adhesion of the PCV is released, the HPFP fuel pressurization process is terminated.

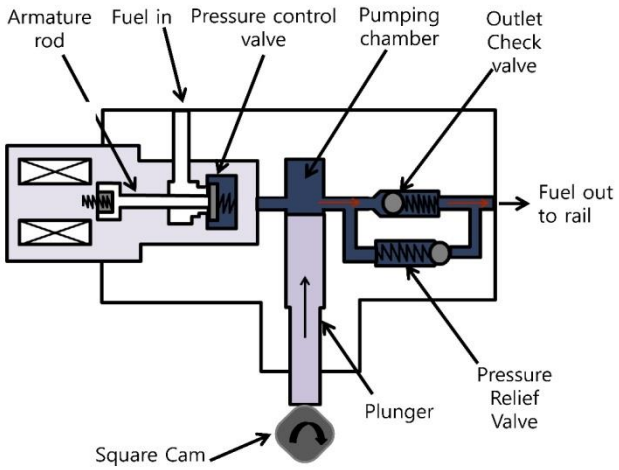


**Figure-1.** Schematic diagram of a GDI high-pressure fuel pump (HPFP) [11].

Figure-3 shows a schematic diagram of the GDI fuel injection system used in the 1-D simulation. The GDI fuel injection system consists of a camshaft, a low-pressure fuel pump, a HPFP, a fuel rail, and four injectors. When the camshaft rotates, the fuel fed from the HPFP is delivered to the fuel rail via an orifice installed to reduce the pressure pulsation. Highly pressurized fuel is injected into the cylinder through the injector under conditions where the FRP (fuel rail pressure) remains constant. Factors that determine the FRP are the square cam rotation speed, the PCV close/open timing and the fuel injection rate. The injector driving process can be summarized as follows. By activating the solenoid in the injector, the needle overcomes the spring force, pushing the needle and lifts. As soon as the needle is lifted, fuel is injected into the cylinder. The diameter of the nozzle hole is 0.19 mm, and there are six holes in the GDI injector used in the simulation.

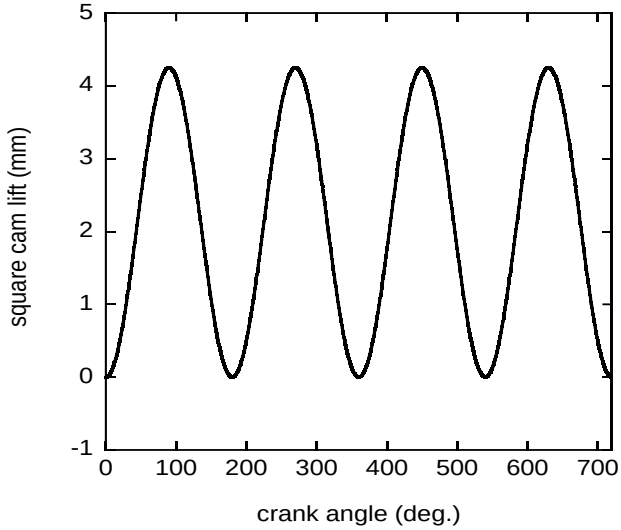


**Figure-2.** GDI square cam lift profile used in this study.

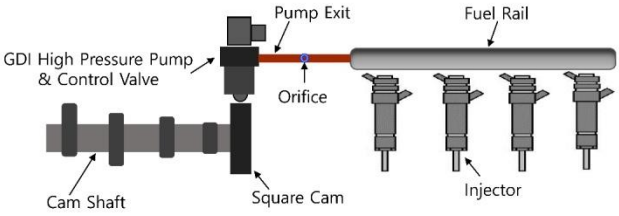


**Figure-3.** A schematic diagram of the GDI fuel injection system used in this study for the 1-D simulation

Three different diameters of the orifice to reduce the HPFP outlet fuel pressure pulsation were used: 0.75, 1.0, and 1.5 mm. The target FRP was simulated for three cases: 50, 100, and 150 bar. Four different engine speeds were used: 1500, 3000, 4500, and 6000 rpm. The fuel injection duration is 1 ms. The fuel pressure pulsation at the HPFP exit shown in Figure-3 was simulated. The pulsation of the FRP was also simulated. For various simulation conditions, the signal-to-noise ratio of the pressure pulsation wave at both the HPFP outlet and the fuel rail was obtained. The optimal PCV closing angle was found to reach the target FRP when varying the opening angle of the PCV from 45 ° BTDC to 60 ° ATDC with a crank angle interval of 15 °. The injected fuel mass per stroke under each simulation condition was also simulated.

**RESULTS AND DISCUSSIONS**

The three main factors which determine the FRP are the PCV closing/opening timing, the engine speed, and the fuel injection rate. For a given engine speed, fuel injection duration and PCV opening angle, the optimal PCV closing angle was obtained to determine the target FRP by a 1-D simulation. The PCV opening angles used in the simulation were changed at 15 ° intervals from 45 ° BTDC (crank angle degrees) to ATDC 60 °. When the PCV is closed, the rail pressure starts to rise. When it is opened, the rail pressure decreases.

Figure-4 shows the simulation results when the PCV closes before opening under various conditions of the

target FRP, orifice diameter, and PCV opening angle at the engine speed of 6000 rpm. In Figure-4, the first, second, third, and fourth points on the x-axis denote the four fuel injections per engine cycle. When the PCV opens earlier than BTDC 45°, the target FRP was not reached in all simulation conditions. Moreover, the target FRP of 150 bar was not reached at PCV opening angles of BTDC 30 ° or BTDC 15° with orifice diameters of 0.75 or 1.0 mm. Overall, the earlier the PCV opening time (the larger the BTDC value), the higher the target FRP, and the smaller the orifice diameter becomes, the more difficult the target FRP control also becomes. Moreover, the PCV closing duration to achieve the target FRP tends to increase as the PCV opening becomes retarder (a larger ATDC value). From the viewpoint of a stable FRP control, the optimal PCV opening angle is preferably after ATDC 15°.

Figure-5 shows the simulation results when the PCV closes before opening under various target fuel rail pressure, orifice diameter, and PCV opening angle conditions at an engine speed of 4500 rpm. The results shown in Figure-5 are similar to those in Figure-4, except that the PCV opening angle to achieve the target FRP was constant under all conditions during the four fuel injections. Simulation results at engine speeds of 3000 rpm and 1500 rpm were similar to those at 4500 rpm.

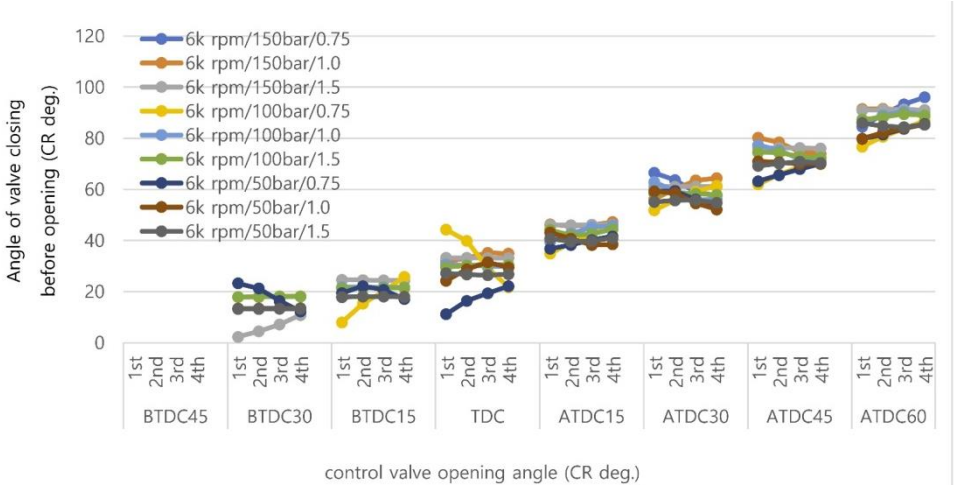


**Figure-4.** PCV valve closing duration with regard to the crank angle (angle of valve closing before opening) according to the various simulation conditions (PCV opening angle, orifice diameter, target FRP, engine speed=6000 rpm) used in this research.

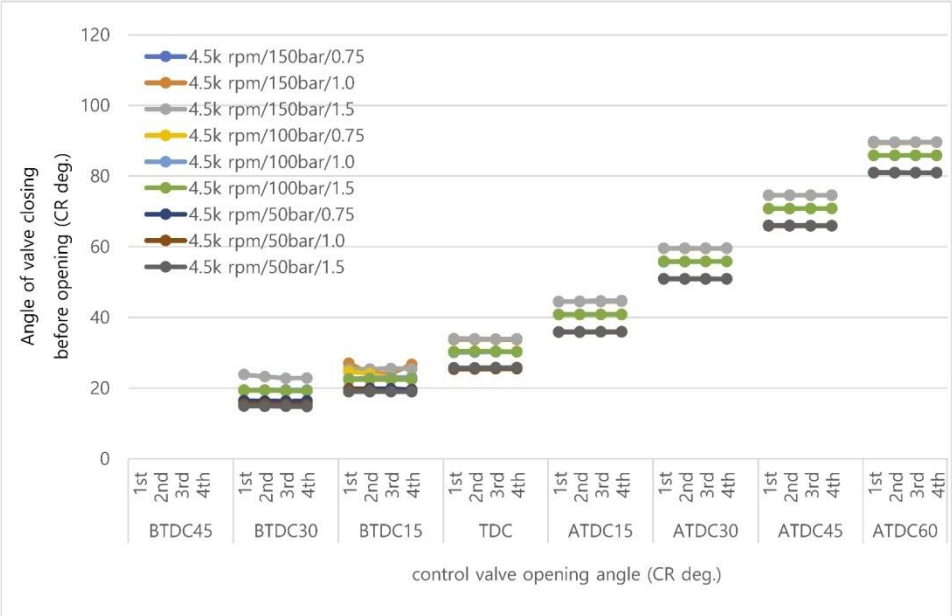


**Figure-5.** PCV valve closing duration with regard to the crank angle (angle of valve closing before opening) according to the various simulation conditions (PCV opening angle, orifice diameter, target FRP, engine speed=4500 rpm) used in this research.

Figure-6 shows an example of the simulation of the fuel pressure at the HPFP outlet. The simulation conditions can be summarized as follows. The target FRP is 150 bar, the engine speed is 3000 rpm, the orifice diameter between the HPFP and the fuel rail is 1.0 mm, and the fuel injection duration is 1 ms. Figure-6 shows the fuel pressure at the HPFP outlet obtained under the various PCV opening angle conditions when the target FRP is reached under the above-mentioned simulation conditions. The pulsation of the fuel pressure at the HPFP outlet was largest when the PCV opening angle was BTDC 30 °. As the PCV opening is delayed, the pulsation tends to decrease gradually. The simulation results shown in Figure-7 were gained when the orifice diameter was 1.5 mm. The simulation results in Figure-7 are very similar to those in Figure-6 at the PCV opening angle of BTDC 30 ° and BTDC 15 °. When the PCV opening angle was after the TDC, the pressure pulsation gradually decreased. Additionally, after the TDC, the pressure pulsation shows a nearly identical value even when the PCV opening angle is increased. These results indicate that when the PCV opening angle is after the TDC, the effect of suppressing the pressure pulsation of the orifice is minimal at the orifice diameter of 1.5 mm.

When the HPFP pressurizes the fuel, it passes through the orifice to fill the fuel rail. Figure-8 shows the simulation results of the FRP pulsation. The simulation conditions in Figure-8 are completely identical to those in Figure-6. Figure-8 shows that the FRP pulsation is greatly reduced after passing through the orifice. At the PCV opening angles of 30 ° BTDC and 15 ° BTDC, the FRP pulsation amplitude was greatly decreased but still showed weak pulsation. In the PCV opening angle range from TDC to ATDC 60 °, almost no FRP pulsation was observed and the FRP pulsation waves were completely identical.

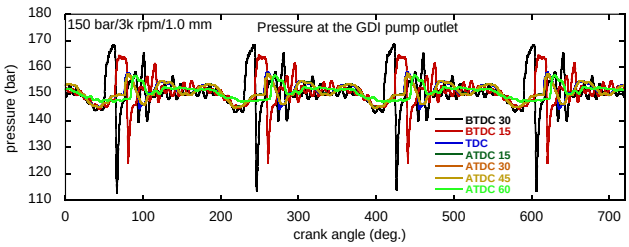


**Figure-6.** Simulation results of the fuel pressure wave at the GDI pump outlet (target FRP=150bar, engine speed = 3000 rpm, orifice diameter=1.0 mm).

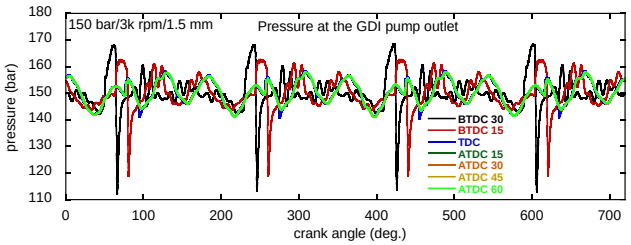


**Figure-7.** Simulation results of the fuel pressure wave at the GDI pump outlet (target FRP=150bar, engine speed = 3000 rpm, orifice diameter=1.5 mm).

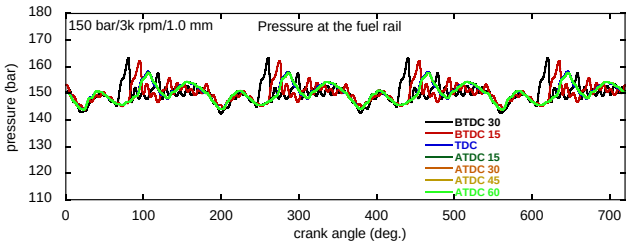


**Figure-8.** Simulation results of the fuel pressure wave at the fuel rail (target FRP=150bar, engine speed = 3000 rpm, orifice diameter=1.0 mm).

Considering the energy consumption when driving the HPFP, it is most advantageous when the PCV closing duration is as short as possible. At the PCV opening angle of BTDC 30 °, the PCV closing duration to drive the HPFP is shortest. The PCV opening angle after the TDC is preferable from the point of view of the variation of the mass of the injected fuel by each injector. Therefore, it is necessary to consider the HPFP driving energy and injected fuel mass variation aspects comprehensively when determining the optimal PCV opening and closing timing of the HPFP.

Figures 6-8 show only a few examples of the fuel pressure pulsation at the HPFP outlet and fuel rail. The signal-to-noise ratio (S/N) was calculated to show the overall pressure pulsation characteristics under the various conditions simulated in this study. The S/N ratio is calculated using the mean (μ) and standard deviation (σ) of the pressure wave signals, as shown in Figures 6-8. The S/N ratio is μ/σ.

Figure-9 shows the S/N ratio of the fuel pressure waves at the HPFP outlet obtained under various simulation conditions. The target FRP was set to 50 bar. The simulated engine speeds are 1500, 3000, and 6000 rpm. The orifice diameters are 1.0 and 1.5 mm. The PCV opening angle was simulated at intervals of 15 ° from BTDC 60° to ATDC 45°. The S/N ratios obtained under the optimum PCV opening angle conditions to achieve the target FRP in each simulation condition are shown. In the PCV opening angle range from BTDC 45° to the TDC, the S/N ratio value tends to increase gradually. After the TDC, the S/N ratio remains nearly constant as the PCV opening angle increases. The larger the S/N ratio is, the smaller the pressure pulsation becomes, indicating that as the PCV

opening angle decreases in the range from BTDC 45 ° to TDC, the pressure pulsation decreases.

Figure-10 shows the S/N ratio of the fuel pressure waves at the HPFP outlet obtained under various simulation conditions when the target FRP is increased to 150 bar. Figure-10 shows results similar to those in Figure-9. The S/N ratio at the HPFP outlet with the target FRP of 150 bar is larger than that at 50 bar.

Figures 11 and 12 show the S/N ratio of the FRP pulsation obtained under the 50 and 150 bar conditions, respectively. Unlike the results in Figures 9-10, the S/N ratio of the FRP pulsation in Figures 11-12 is nearly constant at all the PCV opening angles. The FRP pulsation reduction by the orifice only occurred in the PCV opening angle range from BTDC 45 ° to TDC. Regarding the PCV opening angle after the TDC, the S/N ratio at the HPFP outlet was slightly larger than that at the fuel rail. Generally, when the rail pressure is high, the PCV opening angle is set to be within the BTDC interval, and when the rail pressure is low, it is set after the TDC. Therefore, the pulsation reduction effect by the orifice can be effective only when the rail pressure is controlled to be high.

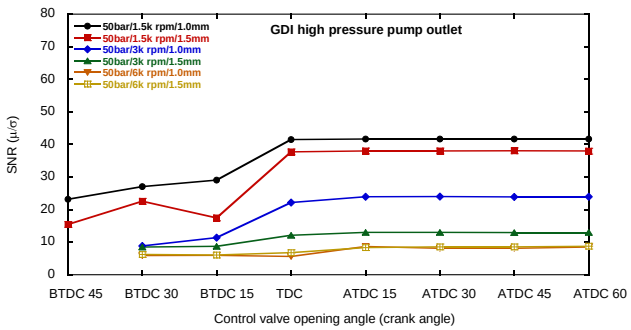


**Figure-9.** Signal-to-noise ratio at the GDI pump outlet (target FRP=50 bar, engine speed = 1500, 3000, 6000 rpm, orifice diameter=1.0, 1.5 mm).

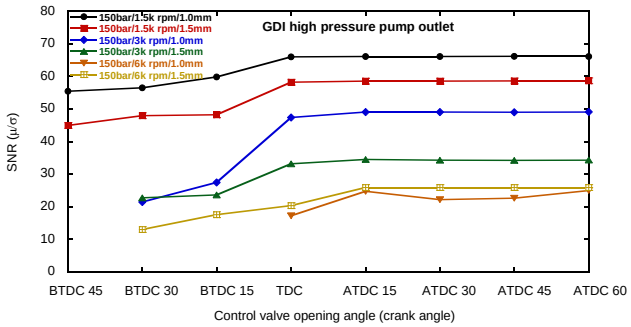


**Figure-10.** Signal-to-noise ratio at the GDI pump outlet (target FRP=150 bar, engine speed = 1500, 3000, 6000 rpm, orifice diameter=1.0, 1.5 mm).

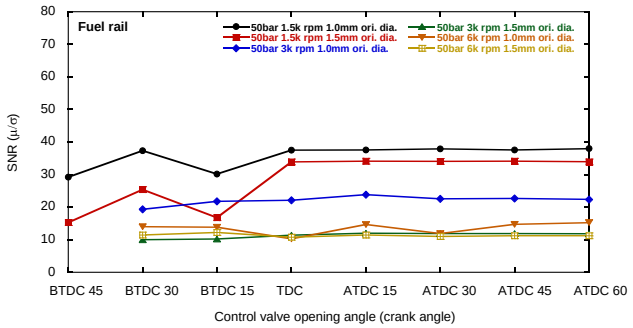


**Figure-11.** Signal-to-noise ratio at the fuel rail (target FRP=50 bar, engine speed = 1500, 3000, 6000 rpm, orifice diameter=1.0, 1.5 mm).

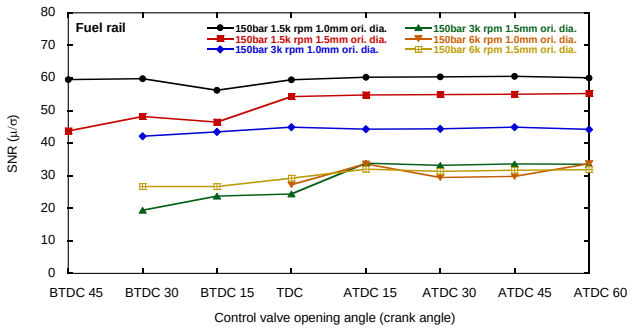


**Figure-12.** Signal-to-noise ratio at the fuel rail (target FRP=150 bar, engine speed = 1500, 3000, 6000 rpm, orifice diameter=1.0, 1.5 mm).

Figure-13 shows the result of simulating the injected fuel mass per injection stroke under various conditions of the target FRP, orifice diameter, and PCV opening timing at the engine speed of 6000 rpm. The first, second, third, and fourth notations on the x-axis indicate the four sequential fuel injections. The characteristics of the injected fuel mass per injection stroke are similar to those in the PCV closing angle simulation for the target FRP shown in Figure 4. The PCV opening angle for the target FRP shows variation of the fuel injection mass per stroke in the range of BTDC 45 to the TDC and a stable injection mass per stroke after the TDC.

Figure-14 shows the simulation results of the injected fuel mass per stroke under various conditions of the target FRP, orifice diameter, and PCV opening angle at the engine speed of 4500 rpm. The injected fuel mass per stroke shows almost no variation over all simulation conditions at the engine speed of 4500 rpm. These results show characteristics similar to those in Figure-5. The characteristics of the injected fuel mass per injection stroke at the engine speeds of 3000 and 1500 rpm were similar to those at 4500 rpm.

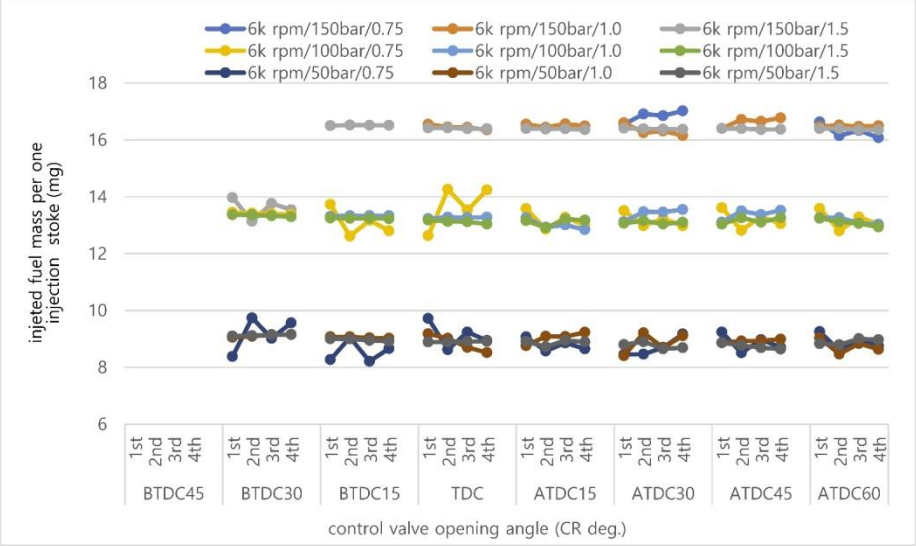


**Figure-13.** Simulation results of injected fuel mass for one injection stroke with various conditions (target FRP=50, 100, 150 bar, orifice diameter=1.0, 1.5mm, engine speed = 6000 rpm).

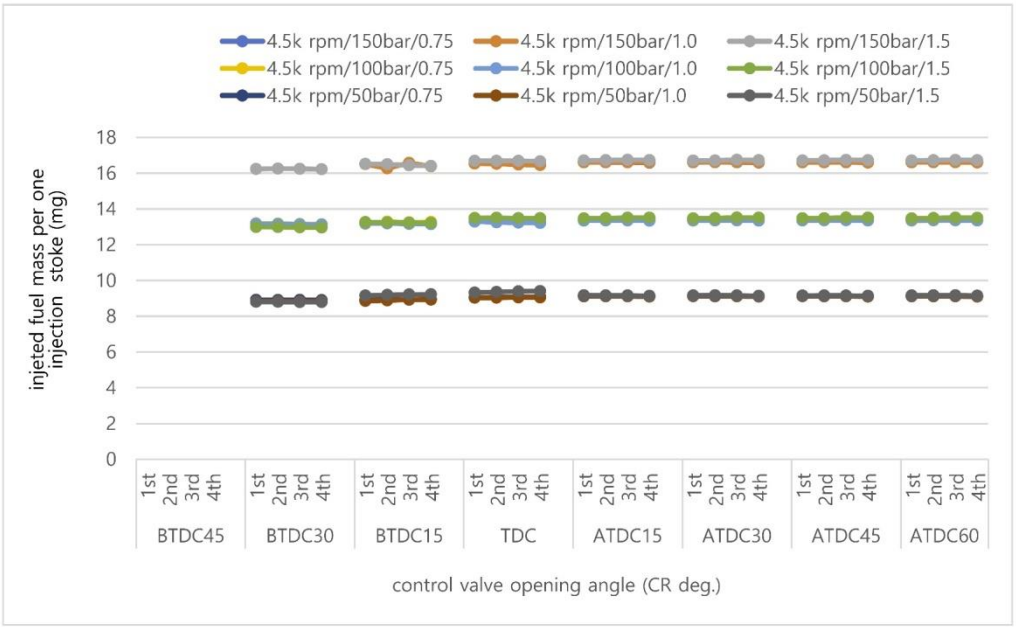


**Figure-14.** Simulation results of injected fuel mass for one injection stroke with various conditions (target FRP=50, 100, 150 bar, orifice diameter=1.0, 1.5mm, engine speed = 4500 rpm).

## CONCLUSIONS

A 1-D simulation of the fuel pressure wave and fuel injection rate from a single-piston type of GDI HPFP driven by a square cam was performed using GT-Suite software. The optimal PCV closing angle before the opening of the PCV was simulated when the PCV opening angle was fixed while varying the engine speed and the orifice diameter between the HPFP outlet and the fuel rail. The following results were obtained.

a) The earlier the PCV opening, the higher the target FRP and the smaller the orifice diameter, making it more difficult to reach the target FRP stably. Moreover, the PCV closing duration to achieve the target FRP tends to increase as the PCV opening is retarded.

b) When the PCV opening angle is after the TDC, the effect of suppressing the pressure pulsation of the orifice is reduced when the orifice diameter increases.

c) When the PCV opening angle is in the range of BTDC 45 to TDC, the S/N ratio tends to increase. The S/N

ratio is constant after the TDC. The larger the S/N ratio is, the smaller the pressure pulsation becomes. This indicates that as the PCV opening angle is retarded in the range of BTDC 45 ° to TDC, the pressure pulsation decreases.

d) The characteristics of the injected fuel mass per stroke are similar to those of the PCV closing angle obtained by the simulation to reach the target FRP.

**REFERENCES**

[1] Reddy A. A. and Mallikarjuna J. M. 2017. Parametric Study on a Gasoline Direct Injection Engine - A CFD Analysis.SAE paper No. 2017-26-0039.

[2] Zhao F. Q. and Lai M. C. 1997. A Review of Mixture Preparation and Combustion Control Strategies for Spark-Ignited Direct-Injection Gasoline Engines. SAE paper No. 970627.

[3] Golzari R., Li Y. and Zhao H. 2016. Impact of Port Fuel Injection and In-Cylinder Fuel Injection Strategies on Gasoline Engine Emissions and Fuel Economy. SAE paper 2016-01-2174.

[4] Zhao F. Q., Lai M. C., and Harrington D. L. 1999. Automotive Spark-Ignited Direct-Injection Gasoline Engines. Progress in Energy and Combustion Science. 25: 437-562.

[5] Um I. 2006. Advanced Internal Combustion Engine. A-Jin Publishing Limited.

[6] Edwin A. Rivera, Noreen Mastro, James Zizelman, John Kirwan and Robert Ooyama. Development of Injector for the Direct Injection Homogeneous Market using Design for Six Sigma, SAE paper 2010-01-0594.

[7] Rivera E. A., Mastro N., Zizelman J., Kirwan J. and Ooyama R. 2010. Development of injector for the direct injection homogeneous market using design for six sigma. SAE Paper No. 2010-01-0594.

[8] Zhao H. 2010. Advanced direct injection combustion engine technologies and development. Cambridge: Woodhead Publishing Limited.

[9] Wang C., Xu H., Herreros J. M., Wang J. and Cracknell R. 2014. Impact of fuel and injection system on particle emissions from a GDI engine. Appl Energy. 132: 178-91.

[10] Payri R., Bracho G., Gimeno J. and Bautista A. 2018. Rate of injection modelling for gasoline direct injectors. Energy Conversion and Management. 166: 424-432.

[11] Spegar T. D., Chang S., Das S., Norkin E. and Lucas R. 2009. An Analytical and Experimental Study of a High Pressure Single Piston Pump for Gasoline Direct Injection (GDi) Engine Applications. SAE paper 2009-01-1504.

[12] Spegar T. D. 2011. Minimizing Gasoline Direct Injection (GDi) Fuel System Pressure Pulsations by Robust Fuel Rail Design. SAE paper 2011-01-1225.

[13] Hiraku K., Tokuo K. and Yamada H. 2005. Development of High Pressure Fuel Pump by using Hydraulic Simulator. SAE paper. 2005-01-0099.